Ye, S. et al. (2023) 1.55-µm sidewall grating DFB lasers integrated with a waveguide crossing for an optical beam forming network. IEEE Photonics Technology Letters, 35(14), pp. 785-788. (doi: 10.1109/LPT.2023.3278880)

https://eprints.gla.ac.uk/298696/

Deposited on: 19 May 2023

Enlighten – Research publications by members of the University of Glasgow
https://eprints.gla.ac.uk

*

1.55-µm Sidewall Grating DFB Lasers Integrated with a Waveguide Crossing for an Optical Beam Forming Network

Shengwei Ye, Xiao Sun, Bocheng Yuan, Peter Read, Pierre Maidment, Yongguang Huang, Ruikang Zhang, Scott Watson, Anthony Kelly, John H. Marsh, *Fellow, IEEE*, and Lianping Hou, *Senior Member, IEEE*

Abstract—**By using asymmetric twin-waveguide technology, a 1.55-µm sidewall grating distributed-feedback(DFB)laser monolithically integrated with a passive waveguide crossing was for the first time demonstrated for an optical beam forming network, which needs only one metalorganic vapor-phase epitaxy step. The DFB laser with uncoated facets presents a side-mode suppression ratio of >44 dB and a low 3-dB linewidth of 68 kHz. An elliptical parabolic taper waveguide crossing had a theoretical crosstalk suppression ratio of 40 dB, while the measured cross-talk suppression ratio was at least 20 dB.**

Index Terms—**DFB laser, asymmetric twin-waveguide, waveguide crossing, laser linewidth.**

I. INTRODUCTION

WITH the rapid development of photonic systems, techniques for manufacturing low cost, multifunctional, high performance, chip-scale photonic integrated circuits (PICs) are necessary. There are three main methods to realize monolithic InP-based PICs with low loss passive waveguides. The most general approach is to use butt-joint regrowth technique [1]-[3], whereas it usually needs complicated and time-consuming etch and regrowth processes. The second method is to use quantum well intermixing (QWI) technology [4]-[6] to modify the quantum well bandgap in selected regions to form a low-loss waveguide at the lasing wavelength of the as-grown wafer. QWI technology is a relatively flexible fabrication route for forming PICs, however careful preparation of the sample and high temperature annealing are required. The third method is to employ asymmetric twin-waveguide (ATG) technology [7]-[9]. Compared with conventional QW laser wafer structures, ATG wafer structures include a low-loss passive waveguide with a lower refractive index beneath the active QW waveguide. Lateral tapers along the active waveguide are used to ensure efficient light coupling between the upper active waveguide and the lower passive waveguide. The ATG technique needs only one metalorganic vapor-phase epitaxy (MOCVD) step and PICs based on ATG technology can be rapidly manufactured by using standardized fabrication processes.

As the complexity of PICs increases, waveguide crossings are inevitably required, and efficient designs are needed, especially for PICs with multiple crossings [10], [11]. To date, most of the waveguide crossings reported in the literature are for silicon-based PICs and are rare for InP-based PICs. In this paper, by using ATG technology, a 1.55-µm sidewall grating (SWG) distributed-feedback laser (DFB) laser monolithically integrated with a passive waveguide crossing is reported for the first time for use in an InP-based optical beam forming network. Conventional DFB lasers with buried gratings use complicated fabrication technologies, including etch and regrowth processes to complete the epitaxy of the laser structure after grating definition. DFB lasers based on SWGs have several advantages, such as regrowth free fabrication processes, increased design flexibility and they readily allow the use of Al-containing epitaxial structures. The gratings can be defined simultaneously with the ridge waveguide, significantly simplifying the device manufacturing process. Compared with conventional regrown butt-joints [3], used for III-V photonic integration, passive waveguides and crossings fabricated by the ATG technique need only a single MOCVD step as described above.

II. DEVICE DESIGN AND FABRICATION

The ATG epitaxial structure is shown in Fig. 1(a). A 1.5 µm-thick undoped InP buffer layer is grown on a semi-insulating InP substrate, followed by three periods of 0.12-µm-thick $In_{0.85}Ga_{0.15}As_{0.33}P_{0.67}$ and 0.4-µm-thick InP stacks, acting as the lower passive waveguide 1, which has a low absorption loss (around 2.8/cm at 1.55-µm wavelength measured by the method described in [12]). Waveguide 2 is the active waveguide and

Shengwei Ye, Xiao Sun, Bocheng Yuan, Peter Read, Pierre Maidment, Scott Watson, Anthony Kelly, Lianping Hou and John H. Marsh are with the James Watt School of Engineering, University of Glasgow, Glasgow G12 8QQ, U.K. (shengwei.ye@glasgow.ac.uk; 2288933s@student.gla.ac.uk; 2644187y @student.gla.ac.uk; p.read.1@research.gla.ac.uk; p.maidment.1@research. gla.ac.uk; scott.watson@glasgow.ac.uk; anthony.kelly@glasgow.ac.uk; john.marsh@glasgow.ac.uk; lianping.hou@glasgow.ac.uk).

Yongguang Huang and Ruikang Zhang are with the Key Laboratory of Semiconductor Materials Science, Institute of Semiconductors, Chinese Academy of Sciences, Beijing 100083, China, and also with the Center of Materials Science and Optoelectronics Engineering, University of Chinese Academy of Sciences, Beijing 100049, China (e-mail: yghuang@semi.ac.cn; rkzhang@semi.ac.cn)
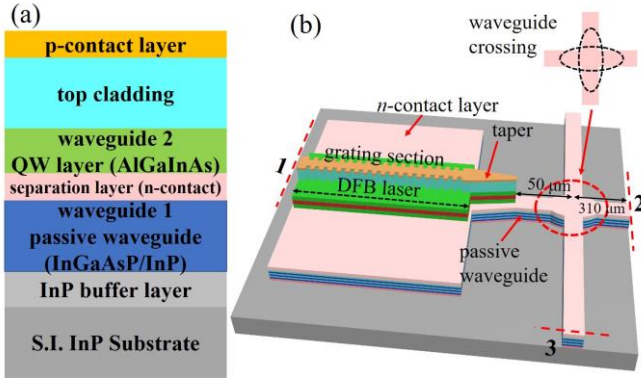
Fig. 1. (a) ATG wafer structure. (b) 3D view of DFB laser integrated with a passive waveguide crossing using the ATG technique.

includes five 6-nm-thick AlGaInAs quantum wells (QW) and six 10-nm-thick AlGaInAs quantum barriers (QB). Its effective refractive index is higher than that of waveguide 1, so in the DFB section, most of the light is confined in waveguide 2. A highly n-doped InP separation layer with a thickness of 0.3 μm is sandwiched between waveguide 1 and waveguide 2, which also acts as an n-contact layer for the laser. The epitaxial structure for the multiple QWs (MQWs) and the upper layers is the same as that described in [13].

Our proposed design of the 1.55-μm DFB laser integrated with a passive waveguide crossing is shown in Fig. 1(b). The width of the grating ridge waveguide is 2.5 μm, with a grating recess depth of 0.6 μm and a grating period of 244 nm. The coupling coefficient κ is measured to be approximately 65 cm^{-1} using the subthreshold spectra-fitting method [14]. At the center of the cavity, a quarter wavelength shift has been introduced to enhance single mode lasing. An exponential taper at the end of the sidewall grating DFB of length 300 μm and whose width is tapered from 2.5 μm to 0.5 μm is defined in waveguide 2. Below this, an exponential taper of the same length, but whose width changes from 6 μm to 2.5 μm, is defined in waveguide 1. These two tapers are used to couple light from the 600-μm-long DFB section to the lower 2.5-μm-wide passive waveguide with good efficiency, simulations show 89% power transfer can be achieved, as shown in Fig. 2(a). When light reaches the waveguide crossing, designed with an elliptical parabolic taper, the light should propagate straight through rather than being coupled into the crossing waveguide or being scattered or reflected. The geometry of the elliptical parabolic taper waveguide crossing comprises two orthogonal ellipses, with major and minor axes of 6 μm and 1.6 μm respectively. The crossing is located 50 μm away from the tip of the upper taper, as shown in Fig. 1(b). Figure 2(b) shows that the simulated cross-talk suppression ratio of this waveguide crossing is around 40 dB at wavelengths around 1.55 μm.

This device structure was fabricated using 3-step dry etch processes with a Cl$_2$/CH$_4$/H$_2$/Ar recipe. First, the p-contact and top cladding layers were etched to form the grating of the DFB laser section and upper taper structure. Then, after protecting the grating section and its two side areas, the structure was etched down to the n-contact separation layer. Last, after
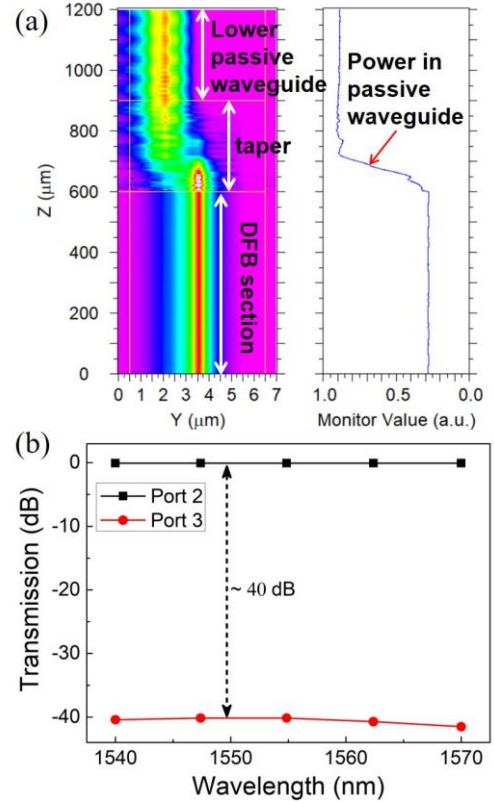

Fig. 2. (a) Simulation of light propagation through the DFB active waveguide to the lower passive waveguide. (b) Simulated light transmission through the waveguide crossing as a function of the wavelength.
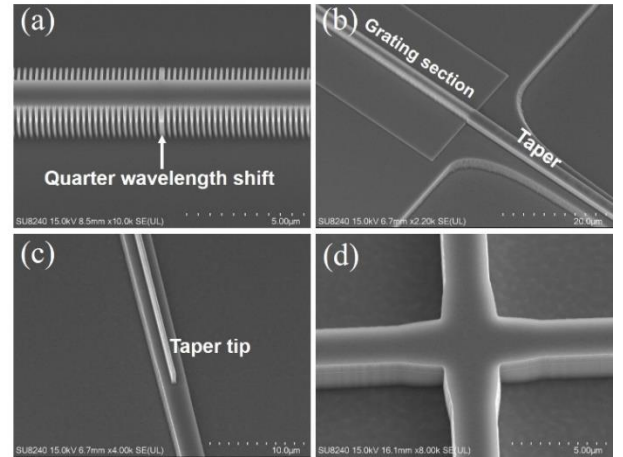

Fig. 3. SEM images of the fabricated DFB grating(a), coupling taper and underneath passive waveguide (b, c), and passive waveguide crossing (d).

defining the n-contact area, the structure was etched through separation layer and waveguide 1, to a depth of 1 μm within the InP buffer layer to create passive waveguides with a height of about 2.88 μm. Figure 3 shows SEM images of the fabricated DFB grating, taper, and passive waveguide crossing after the 3-step dry etch process. Finally, the device was passivated, p- and n-contact windows were opened, and metal deposition and annealing processes were applied to complete the fabrication. The devices were mounted epilayer up on copper heat sinks and measured under CW conditions at 20 °C after cleaving with both facets left uncoated.
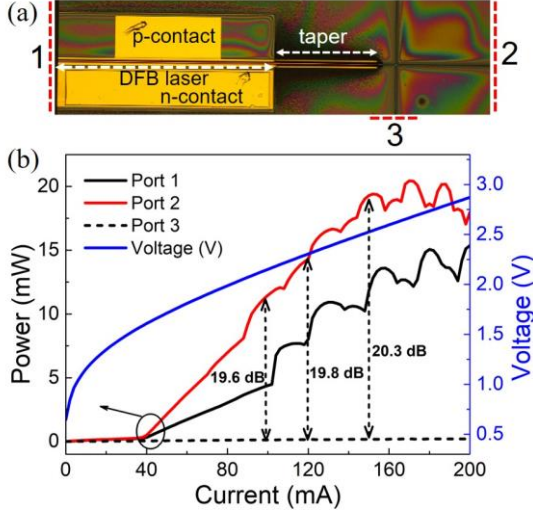
III. DEVICE PERFORMANCE

Fig. 4. (a) Completed device after cleaving. (b) Measured *I-V* and *L-I* characteristic curves.

The completed device is shown in Fig. 4(a). The *p*-contact metal also caps the taper to pump waveguide 2 and reduces absorption loss in the taper section. Port1, port 2, and port 3 represent the output ports at the rear DFB side, waveguide crossing straight through side and crossing side respectively. Optical output powers from port 1, port 2, and port 3 and the current-voltage (*I-V)* characteristics of the DFB laser were measured as shown in Fig. 4(b). The DFB threshold current I_{th} is 36 mA and its ohmic contact resistance is calculated to be 7.58 Ω. The output power from port 2 can reach 20 mW at a DFB current (I_{DFB}) of 170 mA. The ripples or kinks in the light-current (*L-I*) curves are the result of reflections from the taper coupler, waveguide crossing, and uncoated facets, and the phases of these reflections vary with the bias current. The reflection at port 1 should be larger than that from the tip of the taper, and more power will be transmitted in the port 2 direction, which accounts for the output power from port 2 being higher than that of port 1. These results also show the taper structures couple light efficiently from the upper active waveguide to the lower passive waveguide. The output power from port 3 remains at a very low level over the entire measured current range. Based on the measured output power from port 2 and port 3, the calculated cross-talk suppression ratios of the waveguide crossing are 19.6 dB, 19.8 dB, and 20.3 dB at currents of 100 mA, 120 mA and 150 mA respectively. The measured cross-talk suppression ratio is lower than the simulation result of 40 dB, and this was limited by our measurement method. The measured power from port 2 coupled into a lensed fiber is 4.44 mW at I_{DFB} = 100 mA. Since the measured output power from port 3 was too low (only 3~7 nW when I_{DFB} increases from 60 mA to 160 mA) and unstable to measure accurately when using a lensed fiber, a broad area detector (Thorlabs model S132C) was used to collect the power from ports 2 and 3 directly. Taking into account the scattered light in the substrate from port 3, the real output power from the port 3 waveguide should be much less than the measured value, which was confirmed by measuring the power from port 3 using the lensed fiber mentioned above. Therefore, the calculated cross-talk suppression ratio of around 20 dB is an underestimated
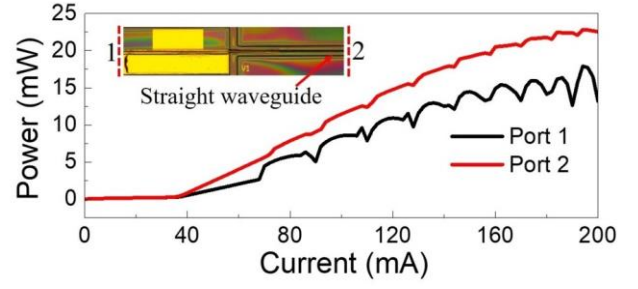

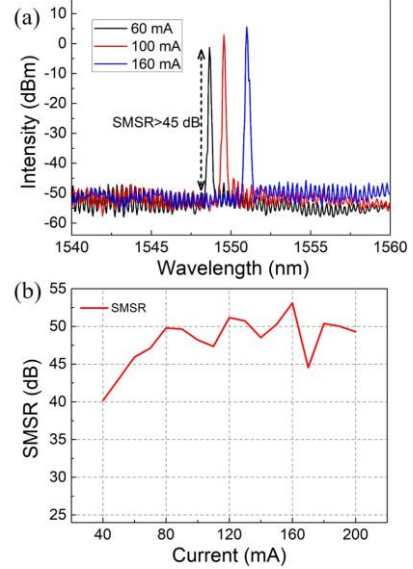Fig. 5. Measured *L-I* characteristic curves for the device with a straight waveguide output port.

Fig. 6. (a) Measured optical spectra from port 2 undercurrents of 60 mA, 100 mA and 160 mA respectively. (b) The measured SMSRs as a function of the current (40 mA to 200 mA).

value. The real cross-talk suppression ratio for the waveguide crossing is therefore larger than 20 dB.

To further investigate the influence of waveguide crossing on laser performance, the *L-I* characteristic curves of devices without waveguide crossing were measured for comparison, as shown in Fig. 5. The trends of the *L-I* curves are about the same as the device that has a waveguide crossing, which verifies again the most light goes straight through the waveguide crossing to the port 2 for the device shown in Fig. 4(a). However, the waveguide crossing shows some additional reflection to the DFB laser, which leads to higher ripples or kinks in the *L-I* curves, as shown in Fig.4(b). By further optimizing the waveguide crossing structure and reducing the reflection from port 2 and port 3, the waveguide crossing additional reflection effect can be greatly mitigated.

The optical spectra from port 2 were measured with a resolution bandwidth (RBW) of 0.06 nm, while the output power from port 3 was too low to be measured. Figure 6(a) shows the optical spectrum at DFB currents of 60 mA, 100 mA, and 160 mA respectively. As can be seen from Fig. 6(a), the lasing wavelength from port 2 is redshifted as the injection current is increased, and the side-mode suppression ratios(SMSRs) for all three currents are larger than 45 dB. The average wavelength redshift was calculated to be 0.031 nm/mA over the current range of 36-200
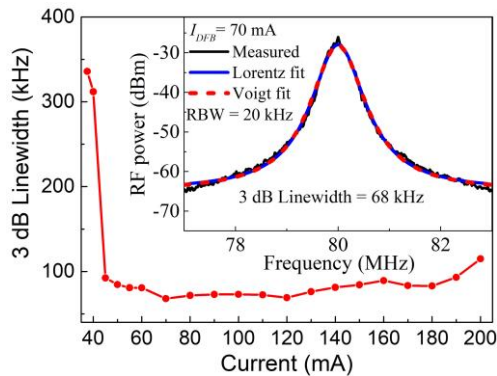
Fig. 7. Measured DFB laser optical spectral linewidth from port 2 as a function of the injection current. The inset shows the measured self-heterodyne beat spectrum (black line) with a Lorenz profile fit (blue line) and Voigt profile fit (red dash line) at I_{DFB}=70 mA.

mA. When I_{DFB} = 100 mA, the peak lasing wavelength is 1549.55 nm with a SMSR = 48 dB. Figure 6(b) shows the SMSRs as a function of I_{DFB}. Over the current range of 40-60 mA, the SMSRs are larger than 40 dB, and when the current was continuously increased from 60 mA to 200 mA, SMSRs larger than 44 dB were maintained.

The optical spectral linewidth from port 2 was measured using a self-heterodyne interferometer setup with an acousto-optic modulator AOM as described in [15], [16]. The length of the delaying fiber was 4.4 km. Lorentz and Voigt profile fittings were used to calculate the 3-dB linewidth of the DFB laser [16], [17]. Figure 7 shows the optical spectral linewidth measured from port 2, and a typical linewidth trend of a DFB laser with power was observed. The linewidth first reduces as I_{DFB} is increased from the threshold current (36 mA) to 70 mA. When $I_{DFB} = I_{th}$, the 3-dB linewidth is 336 kHz. As I_{DFB} increases to 45 mA, the linewidth is reduced to 92.5 kHz. The linewidth reaches the lowest value of 68 kHz at I_{DFB} = 70 mA. When I_{DFB} is increased from 70 mA to 120 mA, the optical linewidth stays nearly constant. When I_{DFB} is increased from 120 mA to 200 mA, the optical linewidth increases slowly and reaches 115 kHz at I_{DFB} = 200 mA. The inset in Fig. 7 shows the narrowest measured self-heterodyne beat spectrum (black line) with good fits to a Lorenz profile (blue line) and a Voigt profile (red dash line) at I_{DFB} = 70 mA. The calculated 3-dB linewidth is 68 kHz. This narrow linewidth may be due to the long cavity length (1260 µm) and the low absorption loss of the passive waveguide. The portion of reflected light from the port 2 facet re-injected back into the DFB cavity will result in a reduction of the linewidth. A linewidth of around 160 kHz was measured for a DFB laser device with a curve waveguide output port, which should be close to the original linewidth of the DFB laser since the facet reflection is suppressed.

IV. CONCLUSION

In summary, an SWG DFB laser monolithically integrated with a passive waveguide crossing using the ATG technique is presented for the first time. With the proper design of the tapers, a high coupling efficiency between the DFB laser section and the lower passive waveguide can be achieved. Single mode operation with SMSRs larger than 44 dB and a narrow

linewidth of 68 kHz can be realized when the DFB laser with uncoated facets. A 20 dB cross-talk suppression ratio was obtained at the waveguide crossing, limited by the sensitivity of the measurement system. This device used SWG and ATG technologies with only one MOCVD step and shows good performance. This fabrication approach is simple compared to wafer regrowth, making it a low-cost and attractive manufacturing route for realizing compact and complex PICs which include multiple monolithic semiconductor lasers and passive crossings.

REFERENCES

[1] M. Suzuki, *et al*., "Monolithic integration of InGaAsP/InP distributed feedback laser and electroabsorption modulator by vapor phase epitaxy," *J. Lightwave Technol.*, vol. LT-5, pp. 1277-1285, Sep. 1987.
[2] P. J Williams, *et al*., "High performance buried ridge DFB lasers monolithically integrated with butt coupled strip loaded passive waveguides for OEIC," *Electron. Lett.*, vol. 26, pp. 142-143, Jan. 1990.
[3] T L. Koch, and U. Koren, "Semiconductor photonic integrated circuits," *IEEE J. Quantum Electron.*, vol. 27, no. 3, pp. 641-653, Mar. 1991.
[4] J. H. Marsh, "Quantum well intermixing," *Semicond. Sci. Technol*., vol. 8, no.6, p. 1136, Feb. 1993.
[5] A. McKee, *et al*., "Monolithic integration in InGaAs-InGaAsP multiple-quantum-well structures using laser intermixing," *IEEE J. Sel. Topics Quantum Electron.*, vol. 33, no. 1, pp. 45-55, Jan. 1997.
[6] E. J. Skogen, *et al*., "Monolithically integrated active components: a quantum-well intermixing approach," *IEEE J. Sel. Topics Quantum Electron.*, vol. 11, no. 2, pp.343-355, Mar. 2005.
[7] V. M. Menon, F. Xia, and S. R. Forrest, "Photonic integration using asymmetric twin-waveguide (ATG) technology: part II-devices," *IEEE J. Sel. Topics Quantum Electron.,* vol. 11, no. 1, pp. 30-42, Jan. 2005.
[8] P. V. Studenkov, M. R. Gokhale, and S. R. Forrest, "Efficient coupling in integrated twin-waveguide lasers using waveguide tapers," *IEEE Photon. Technol. Lett.*, vol. 11, no. 9, pp. 1096-1098, Sep. 1999.
[9] L. Hou, *et al*., "Monolithically integrated laser diode and electroabsorption modulator with dual-waveguide spot-size converter input and output," *Semicond. Sci. Technol.*, vol. 20, no. 8, pp. 779-782, Jun. 2005.
[10] H. Liu, *et al*., "Low-loss waveguide crossing using a multimode interference structure," *Opt. Commun.*, vol. 241, pp. 99-104, Jul. 2004.
[11] M. Smit, *et al*., "An introduction to InP-based generic integration technology," *Semicond. Sci. Technol.*, vol. 29, p. 083001, Jun. 2014.
[12] S. Taebi, *et al*., "Modified Fabry–Perot interferometric method for waveguide loss measurement," *Appl. Opt.*, vol. 47, no. 35, pp. 6625-6630, Dec. 2008.
[13] L. Hou, *et al*., "Low divergence angle and low jitter 40 GHz AlGaInAs/InP 1.55 µm mode-locked lasers," *Opt. Lett.*, vol. 36, no. 6, pp. 966-968, Mar. 2011.
[14] T. Nakura and Y. Nakano, "LAPAREX-An automatic parameter extraction program for gain- and index-coupled distributed feedback semiconductor lasers, and its application to observation of changing coupling coefficients with currents," *IEICE Trans. Electron*., vol. E83-C, no. 3, pp. 488–495, 2000.
[15] H. Ludvigsen, M. Tossavainen, and M. Kaivola, "Laser linewidth measurements using self-homodyne detection with short delay," *Opt. Commun.*, vol. 155, pp. 180-186, Oct. 1998.
[16] S. Huang, *et al*., "Precise measurement of ultra-narrow laser linewidths using the strong coherent envelope," *Sci. Rep.*, vol. 7, no. 1, pp. 1-7, Feb. 2017.
[17] L. B. Mercer, "1/f frequency noise effects on self-heterodyne linewidth measurements," *J. Light. Technol.*, vol. 9, no. 4, pp. 485-493, Apr. 1991.